Journal of Power Sources 194 (2009) 1156–1163

Contents lists available at ScienceDirect

Journal of Power Sources

journal homepage: www.elsevier.com/locate/jpowsour

Thermal behavior of a weatherproof power supply system with built-in nickel-metal hydride batteries developed for stationary use

Akihiro Miyasaka*, Riichi Kitano, Akira Yamashita, Takahisa Shodai

NTT Energy and Environment Systems Laboratories, NTT Corporation, 3-1, Morinosato Wakamiya, Atsugi, Kanagawa 243-0198, Japan

ARTICLE INFO

Article history:
Received 31 March 2009
Received in revised form 2 June 2009
Accepted 8 June 2009
Available online 16 June 2009

Keywords:
Nickel-metal hydride battery
Weatherproof power supply
Backup
High-temperature operation
Thermal design
Generated heat

ABSTRACT

The thermal design of weatherproof power supply system has been evaluated by experiments and simulation. Nickel-metal hydride batteries developed for stationary use were employed in the system due to their high charge/discharge performance in high-temperature environments. As the weatherproof power supply system has a sealed cabinet, we evaluated the temperature characteristics of the battery in a 40 °C environment. In order to predict the temperature of the power system, it was necessary to obtain the rate of heat generation from the battery. For this purpose, we developed an estimation method in which the measured temperature of the battery is approximated as a function of cubic spline interpolation. The temperatures of critical items mounted in the system were calculated on the basis of the experimental results. This paper describes the procedure for estimating the heat generation rate of the battery and the temperature of the system. Our results show that the weatherproof power system is useful for operation in high-temperature environments.

1. Introduction

Over the past several years, many natural calamities have struck globally and caused severe damage. Prompt and accurate information about the circumstances in emergencies is necessary so that government or public services can respond quickly and effectively. In addition to gathering and sending information, measures must be taken to ensure safety and security in emergencies. One of the important challenges is how to ensure electricity when disasters cause a breakdown of utilities.

Power supply systems with valve regulated lead acid batteries (VRLABs) are commonly used as backup power systems or uninterruptible power systems (UPSs). Many public offices have prepared stationary backup power supply systems with VRLABs, because their robust charge–discharge characteristics, many proven technologies, and low cost provide an economical, stable power source and a safe and secure system.

Recently, systems for acquiring field data and images through monitoring systems and public radio systems have figured more prominently in emergencies. With conventional systems, the backup duration is several hours. Though longer operation times for power systems for outdoor use in emergencies are desired, it is difficult to increase the volume of VRLABs because of their low energy density. Moreover, the components of the power supply systems for outdoor use, including the batteries, are housed in a sealed cabinet to protect them from the elements and corrosion by gases. The temperatures of the components become especially high in summer. Operating VRLABs in high-temperature atmosphere leads to accelerated deterioration and damage. Therefore, a battery cooling system in the closed cabinet is indispensable. On the whole, the lifespan of VRLABs in stationary power systems for outdoor use is shorter than for indoor use.

To overcome these shortcomings of VRLABs, we have developed a nickel-metal hydride (Ni-MH) battery for backup use by changing the material of the electrodes and the composition and concentration of the electrolyte [1,2]. The energy density is approximately three times greater than that of VRLABs. The capacity of the developed Ni-MH battery is 95 Ah in a cylindrical shape, and high charge and discharge performance can be achieved under high ambient temperatures. The life of the battery is expected to exceed 8 years under use in 40 °C environments, whereas the life expectancy of VRLABs in such environments is less than 5 years. It is important to perform a thermal analysis of a stationary power supply system with the new Ni-MH battery because the high-density mounting system induces high-density heat spots. The operating temperature dependence of battery life must be estimated. Consequently, the economically competitive potential can be evaluated on the basis of the battery life.

Currently, the temperature of electronic equipment for outdoor use is controlled by thermal control devices, such as cooling fans and heat exchangers, on the basis of a thermal analysis [3,4]. Several methods for estimating the heat generated from batteries have

* Corresponding author. Tel.: +81 46 240 2686; fax: +81 46 270 2702.
E-mail address: miyasaka@aecl.ntt.co.jp (A. Miyasaka).

0378-7753/$ – see front matter © 2009 Elsevier B.V. All rights reserved.
doi:10.1016/j.jpowsour.2009.06.014

Nomenclature

A_a	outlet area of cooling air from battery module (m^2)
A_b	surface area of battery (m^2)
A_c	inner surface area of the chassis of battery module (m^2)
A_i	surface area of inverter (m^2)
A_{ia}	outlet area of cooling air from inverter (m^2)
A_p	area of a side panel of system (m^2)
C	geometric parameter
Cp_a	heat capacity of cooling air in battery module ($J K^{-1}$)
Cp_b	heat capacity of battery ($J K^{-1}$)
Cp_c	heat capacity of chassis of the battery module ($J K^{-1}$)
Cp_i	heat capacity of inverter ($J K^{-1}$)
Cp_s	heat capacity of system ($J K^{-1}$)
cp_a	heat specific capacity of air ($J K^{-1} kg^{-1}$)
F	view factor
Gr	Grashof number
g	acceleration of gravity ($m s^{-2}$)
h	heat-transfer coefficient ($W m^{-2} K^{-1}$)
h_{ac}	heat-transfer coefficient between chassis and cooling air ($W m^{-2} K^{-1}$)
h_{ba}	heat-transfer coefficient between battery and cooling air ($W m^{-2} K^{-1}$)
$h_{c\infty}$	heat-transfer coefficient between chassis and ambience ($W m^{-2} K^{-1}$)
h_i	heat-transfer coefficient between inverter and inner air ($W m^{-2} K^{-1}$)
h_s	heat-transfer coefficient between system and ambience ($W m^{-2} K^{-1}$)
I	solar radiation intensity ($W m^{-2}$)
k_a	heat-transfer conductivity of air ($W m^{-1} K^{-1}$)
m	exponent value in Eq. (5)
n	exponent value in Eq. (5)
Nu	Nusselt number
Pr	Prantdl number
Q_{grd}	heat input rate from ground (W)
Q_i	generated heat from inverter (W)
Q_{in}	generated heat from system (W)
Q_{rad}	heat removal to ambient by radiation (W)
Q_{sol}	heat input rate due to solar (W)
q_{in}	generated heat from battery (W)
Re	Reynolds number
T_a	temperature of cooling air in battery module (K)
T_b	temperature of battery (K)
T_{bi}	temperature of battery at time t_i (K)
T_c	temperature of chassis (K)
T_g	temperature of ground (K)
T_i	temperature of inverter (K)
T_s	temperature of system (K)
T_∞	temperature of ambience (K)
t	time (s)
u_a	velocity of cooling air of battery module ($m s^{-1}$)
u_i	velocity of cooling air of inverter ($m s^{-1}$)
x	characteristics dimension (m)

Greek symbols

α_s	solar absorptivity of surface of system
β	volume expansion coefficient (K^{-1})
ε	emissivity of surface of system
θ	solar incident angle from normal direction of surface (°)
ν_∞	kinematic viscosity ($m^{-2} s^{-1}$)
ρ_a	density of air ($kg m^{-3}$)
σ	Stefan–Boltzmann constant ($W m^{-2} K^{-4}$)
τ_{pg}	transfer factor between system panel and ground

been proposed thus far. Practical measurement of the heat generated from VRLABs for hybrid electric vehicles has been performed by using a specially manufactured calorimeter [5]. Moreover, the heat generation rate of VRLABs has been calculated by considering chemical reactions between solution water and oxygen at electrodes [6,7]. For Ni-MH batteries, applications for hybrid electric vehicles and space-related onboard equipment have been studied because the conventional Ni-MH battery was designed for deep-cycle use [8,9]. Only a couple of papers have presented Ni-MH batteries for stationary applications [10,11]. The battery units in those studies were equipped with cooling measures, which were determined by considering the system configuration. Waste heat from the battery has not been entirely clarified.

In this study, the thermal characteristics in the charge–discharge state were obtained by experiment. In order to evaluate the heat generation rate of the Ni-MH battery, we devised an estimation method that uses spline interpolation based on the battery temperature. From the results of the estimation, the temperature on the weatherproof power supply system with built-in Ni-MH batteries was predicted and compared with experimental results.

2. Ni-MH battery and system

2.1. Ni-MH battery and batty module

The Ni-MH battery can be charged and discharged efficiently at more than 40 °C. Table 1 shows the features of the developed Ni-MH battery cell and module, in which 10 cells connected in series, a cooling fan, and an electric connector are installed.

The design concept of the module was developed for convenience of use. The advantages of the battery module are as follows: (i) It is possible to control temperature of the batteries independently by the cooling fan built into the module. (ii) It is easy to change the output power capacity by coordinating the number of battery modules according to requirements. (iii) It should be safer with easier and faster assembly than the VRLAB assembly due to the cartridge-type connector. The battery module is shown in Fig. 1.

2.2. Weatherproof power supply system

A photograph of Ni-MH battery-mounted weatherproof power supply system is shown in Fig. 2.

The system consists of an electrical unit and battery unit. The electrical unit contains an inverter, a charger, an AC switch, and

Table 1
Specification of Ni-MH battery cell and module.

Battery cell	
Nominal capacity	95 Ah
Nominal voltage	1.2 V
Dimension	61 mm in diameter; 175 mm in length
Weight	1.6 kg
Energy density	71 Wh kg^{-1}; 223 Wh L^{-1}
Operation temperature	−10 to 65 °C
Battery module	
Configuration	Ten battery cells connected in series cooling fan, connecter
Dimension	215 mm (*W*), 163 mm (*H*), 430 mm (*D*)
Weight	20 kg
Cooling fan operation	During charging, or over 45 °C in discharging

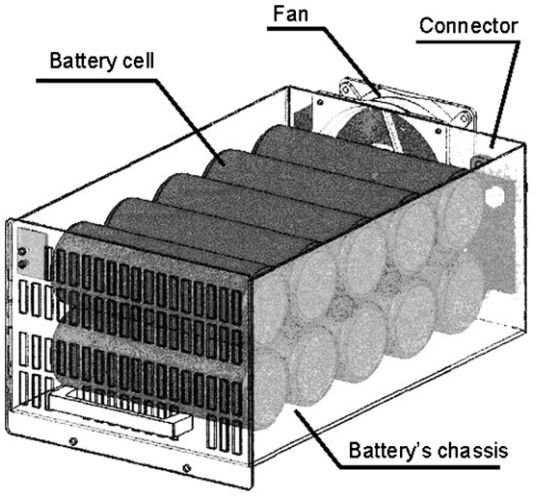

Fig. 1. Battery module constructed of Ni-MH battery cells, cooling fan, and electric connector. A temperature sensor is attached to the battery cell.

Fig. 2. Weatherproof power supply system within Ni-MH batteries. The system can accommodate up to three battery modules, depending on the requirements.

a controller and is mounted above the battery unit. The battery unit can accommodate up to three battery modules depending on required loading power, where at the maximum battery capacity of the system is 3.4 kWh. Since the nominal load power is 150 VA (200 VA is the maximum specification value), the backup duration can reach 20 h with a 3-module mount. Specification of the weatherproof power system is shown in Table 2. Commercial power can be delivered through the electrical unit at ordinary times. If utility power goes out, backup power is provided by the battery unit just after the operation of a high-speed semiconductor switch, i.e., an AC switch, within a 10 ms switchover time.

Table 2
Specification of weatherproof power supply system.

Proposed	
Battery type	Ni-MH
Output power (nominal)	150 VA
Backup duration	20 h
Weight	130 kg
Volume	0.223 m^3
Life expectancy	8 years at 45 °C

Table 3
Heat generation rates and allowable upper temperature.

	Heat generation rates	Remarks
Inverter	47 W (at 200 VA)	65 °C (allowable upper temperature)
Battery	40 W (max), 1-module 20 W (max), 2-module 11 W (max), 3-module	65 °C (allowable upper temperature) (calculation of heat generation is shown in next section)

We estimated the temperature of the inverter and battery module in discharging state. The inverter generates most of the waste heat in the electrical unit. The charger also generates waste heat, but it is only operated a short time and infrequently, about a half and hour a month. The battery is supposed to be charged when its capacity decreases by 90% due to self-discharge; that is, battery is charged when the state of charge (SOC) becomes 90%. Thus, we regard the charger as a non-critical item in the thermal evaluation. The cabinet housing the system is sealed for protection from rain or harmful gases. Meanwhile, the heat from the equipment can only dissipate through the four panels of the cabinet, so that it is difficult to remove waste heat in the system. Table 3 shows the heat generation rates and the design temperature of the equipment during discharge. The heat generation rate of the inverter can be calculated by efficiency in discharging; however, the heat from the battery must be estimated.

Table 3 lists three heat generation rates when one, two, or three battery modules are mounted, i.e., 1-module, 2-module, and 3-module condition. One battery module loaded in the system is the most critical condition for thermal evaluation, because the discharge current concentrates in a single battery module. Accordingly, the amount of ohmic heating also becomes greater. Therefore, we focus in this paper on the thermal characteristics for 1-module mounting.

The thermal design points of the weatherproof power supply system are as follows:

(1) The surface of the cabinet coated with infrared reflecting paint.
(2) A sun shield over the roof of the cabinet.
(3) Operation of the cooling fan built in the inverter by thermostatical control with any of the following conditions:
  (i) The temperature of the inverter rises over 50 °C.
  (ii) The temperature of the atmosphere near the inverter is over 40 °C.
(4) Operation of the cooling fan built in the battery module when temperature is over 45 °C in discharging. This battery was designed so as not to exceed the allowable upper temperature, i.e., 65 °C, to prevent thermal runaway. We determined the temperature of fan drive start within a sufficient margin.

3. Heat generation rate from battery

3.1. Method for estimating heat generated from battery

It is difficult to measure the heat generated from a battery in the operating condition. Thus, we propose an estimation method based on the measured battery temperature. The amount of the heat from the battery is derived from the cubic spline interpolation of temperature measured empirically in discharging. The difference in temperature among the battery cells in the module is within 3 °C, so we regard the heat generated from the battery module as one analysis element. The bulk temperature for the analysis is

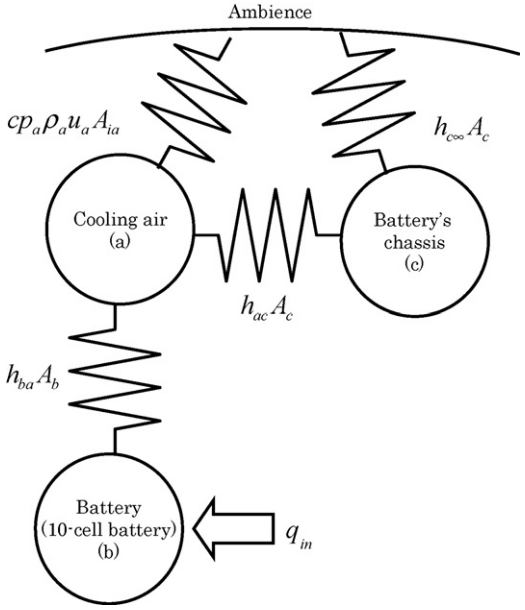

Fig. 3. Thermal mathematical model of the battery module for calculating the heat generation rate. This model was developed under the condition of driving the cooling fan.

represented as the average temperature of the 10 battery cells in the module. A thermal mathematical model of the battery module was built on the basis of the experimental configuration. The temperatures were measured under the condition of battery module testing in discharging. In actual operation of the power system, the cooling fan built into the module activates only when the temperature exceeds 45 °C in discharge. However, in this work, the fan was operated continuously during discharge because the heat dissipation rate was calculated from velocity of the air and temperature difference between inlet and outlet flows.

We adopted a nodal method for the temperature analysis of the battery. The thermal mathematical model in the nodal method is shown in Fig. 3.

The analysis model for the battery module consists of the battery, the cooling air, and the battery chassis. The thermal equilibrium equations are:

$$\mathrm{Cp_b}\frac{dT_\mathrm{b}}{dt} + h_\mathrm{ba}A_\mathrm{b}(T_\mathrm{b} - T_\mathrm{a}) - q_\mathrm{in} = 0 \tag{1}$$

$$\mathrm{Cp_a}\frac{dT_\mathrm{a}}{dt} + h_\mathrm{ba}A_\mathrm{b}(T_\mathrm{a} - T_\mathrm{b}) + \mathrm{cp_a}\rho_\mathrm{a}u_\mathrm{a}A_\mathrm{ia}(T_\mathrm{a} - T_\infty) + h_\mathrm{ac}A_\mathrm{c}(T_\mathrm{a} - T_\mathrm{c}) = 0 \tag{2}$$

$$\mathrm{Cp_c}\frac{dT_\mathrm{c}}{dt} + h_\mathrm{ac}A_\mathrm{c}(T_\mathrm{c} - T_\mathrm{a}) + h_{\mathrm{c}\infty}A_\mathrm{c}(T_\mathrm{c} - T_\infty) = 0 \tag{3}$$

The above equations include the convection heat-transfer coefficients, h_ba, h_ac, $h_{\mathrm{c}\infty}$, which are expressed by using Nusselt number, *Nu*, as

$$Nu = \frac{hx}{k_\mathrm{a}} \tag{4}$$

The Nusselt number is generally expressed as a function of Reynolds number, *Re*, and Prandtl number, *Pr*, as

$$Nu = C\ Re^m Pr^n \tag{5}$$

The second term is Eq. (1) expresses heat removal from the battery by cooling air. The convection heat-transfer coefficient, h_ba, was determined based on heat-transfer characteristics of multi rows of tubes. The battery has an assembly structure of a bank of tubes, two rows high and five rows deep. Following Ref. [12], geometry parameter *C* and exponent values *m* and *n* in Eq. (5) were determined from the number of the tubes and their dimensions and arrangement. The fourth term in Eq. (2) indicates heat exchange between the cooling air and battery chassis. The heat-transfer coefficient, h_ac in forced convection through a rectangular tube was estimated from the empirical relation for pipe and tube flow [12] as shown in Eq. (5). The geometry parameter *C* and exponent values *m* and *n* used in this estimation are shown in Table 4.

Table 4
Heat-transfer coefficient in Eq. (5).

Parameter in Eq. (5)	h_ba	h_ac
C	0.254	0.023
m	0.632	0.8
n	1/3	0.3

The third term in Eq. (3) is the heat transfer between the battery chassis and ambience. The heat-transfer coefficient $h_{\mathrm{c}\infty}$ was used as the natural-convection heat transfer. The Nusselt number for natural-convection heat transfer can be rewritten as a function of Grashof number *Gr* as

$$Nu = \frac{h_{\mathrm{c}\infty}x}{k_\mathrm{a}} = C(Gr\ Pr)^{1/4} \tag{6}$$

$$Gr = \frac{g\beta(T_\mathrm{c} - T_\infty)x_\mathrm{c}^3}{\nu_\infty^2} \tag{7}$$

If the heat transfer is natural convection on vertical planes, geometric parameter *C* is assigned a value of 0.59. Meanwhile, 0.54 is assigned to *C* if on the upper surface of heat plates or lower surface of cooling plates [13]. β is equal to the reciprocal of the average of temperatures of the chassis and ambience.

The third term in Eq. (2) describes the rate of heat of outflow to the ambient by cooling air. The cooling velocity u_a is the average of the measured data. The flow area, A_ia, is defined as outlet area of the battery module.

In the conventional temperature calculation, the temperatures in Eqs. (1)–(3) are numerically solved when the heat generation rate, q_in, is given. Conversely, the heat generation rate is obtained if the temperature of the battery module T_b can be given as a function of time. Therefore, we assumed that the temperature is approximated as a cubic spline function. The cubic spline function was chosen because the spline interpolation is stabilized for solving the

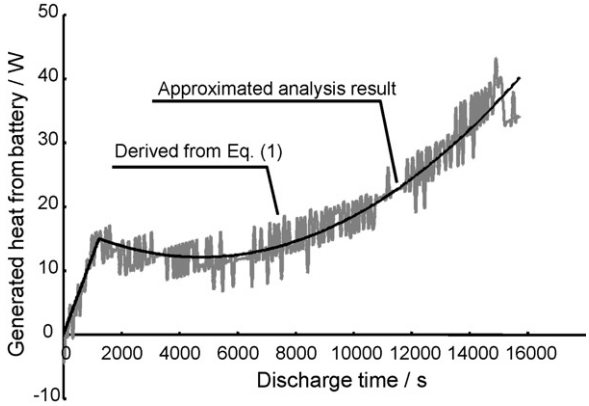

Fig. 4. Rate of heat generation from battery. The thin line shows raw numerical values calculated using Eqs. (1)–(3). The heavy line shows the polynomial approximation for the raw numerical values.

equations and because it is difficult to obtain other approximations passing through several measured data and boundary conditions. Then, the spline interpolation can express the second-order derivative.

The cubic spline function is expressed by a function of time between $[t_i, t_{i+1}]$.

The cubic spline function is described as

$$T_b(t) = c_0 + c_1(t - t_i) + c_2(t - t_i)^2 + c_3(t - t_i)^3 \quad (8)$$

where c_0, c_1, c_2, and c_3 are coefficients of the cube spline function. Eq. (8) can be rewritten as

$$T_b(t) = T_{bi} + \left[\frac{T_{bi+1} - T_{bi}}{h_i} - \left(\frac{w_i}{3} + \frac{w_{i+1}}{6}\right) h_i\right](t - t_i) + \frac{w_i}{2}(t - t_i)^2 + \left[\frac{w_{i+1} - w_i}{6h_i}\right](t - t_i)^3 \quad (9)$$

where $h_i = t_{i+1} - t_i$, and w_i is the second-order derivative of T_b and expressed as

$$[w_2, w_3, \ldots, w_{n-1}]^T = 6\begin{bmatrix} 2(h_1 + h_2) & h_2 & & \\ h_2 & 2(h_2 - h_3) & h_3 & \\ & \cdots & & h_{n-2} \\ & h_{n-2} & 2(h_{n-2} + h_{n-1}) & \end{bmatrix}^{-1} \begin{bmatrix} \frac{T_3 - T_2}{h_2} - \frac{T_2 - T_1}{h_1} \\ \frac{T_4 - T_3}{h_3} - \frac{T_3 - T_2}{h_2} \\ \vdots \\ \frac{T_n - T_{n-1}}{h_{n-1}} - \frac{T_{n-1} - T_{n-2}}{h_{n-2}} \end{bmatrix} \quad (10)$$

The differentiation of the T_b is written as

$$T'_b = \frac{T_{bi+1} - T_{bi}}{h_i} - \left(\frac{w_i}{3} + \frac{w_{i+1}}{6}\right) h_i + w_i(t - t_i) + 3\left[\frac{w_{i+1} - w_i}{6h_i}\right](t_i - t)^2 \quad (11)$$

T_a and T_c are derived from Eqs. (2) and (3) by substituting Eq. (9). Then, the heat generation rate for the battery module is consequently obtained by Eq. (1).

3.2. Experimental results on heat generation rate

In actual operation, the power system prepares for emergencies in the charging condition on a daily basis. We must verify in discharging whether the system demonstrates appropriate performance even in high-temperature environments. Thus, it is necessary to estimate the amount of heat from the battery to predict the temperature of the power system. The amount of heat from the battery is calculated according to Eqs. (1)–(11). Discharge of the battery module (shown in Fig. 1) was carried out to compare analysis results with experimental data.

The battery was provided 20 A at constant current in discharging under a room-temperature environment. The temperature of the battery obtained as the average of the 10 battery cells in the module was interpolated by the cubic spline function to calculate the heat generation rate. The heat generation rate calculated on the basis of the temperature is shown in Fig. 4.

At the beginning of discharge start at about 2000 s, the heat generation increased linearly. However, the heat profile changed approximately at 2000 s. We are investigating this phenomenon using overpotential resistance.

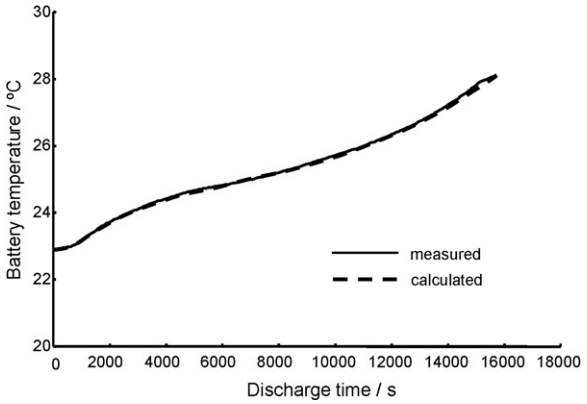

Fig. 5. Battery temperatures in discharging. The solid line shows measured data. The broken line is derived from Eqs. (1) and (2) substituted into the approximated heat generation rate.

The thin line represents raw values derived numerically from the equations, and the bold line shows the result of polynomial approximation for the raw values. The battery temperature was estimated by substituting the polynomial approximated heat rate into Eqs. (1)–(3) to verify this calculation scheme. Fig. 5 shows the comparison temperature between measured data (solid line) and analysis result (broken line).

The measured data agree well with the analysis result. Therefore, it was clarified that the heat generation rate can be estimated from the approximation of temperature by the cubic spline function. Fig. 6 shows the charging voltage, temperature, and heat generation rate.

The discharge was carried out until the voltage reached 10 V. The heat removal by the cooling air was empirically obtained by measuring the velocity of the cooling air at the outlet and the temperature difference of the cooling air between the outlet and inlet. This heat corresponded to the values derived by the third term in Eq. (2). Fig. 7 compares the experimental and measured results. The difference between them was 2 W at maximum. The measured cooling air velocity fluctuated within 0.4 m s^{-1}. This velocity of the variable corresponded to fluctuation of 3 W in wasted heat. Therefore, because the heat removal rate using the analysis was within the allowable fluctuation range, we concluded that the thermal mathematical model of the battery module is sufficient for estimating the heat generation rate of the battery.

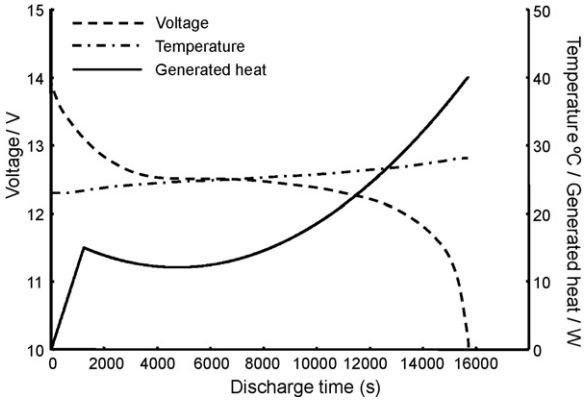

Fig. 6. Discharge characteristics of the battery module. The solid line shows calculated heat generation rate. The broken line shows the measured voltage of the battery module. The chain line shows measured temperature.

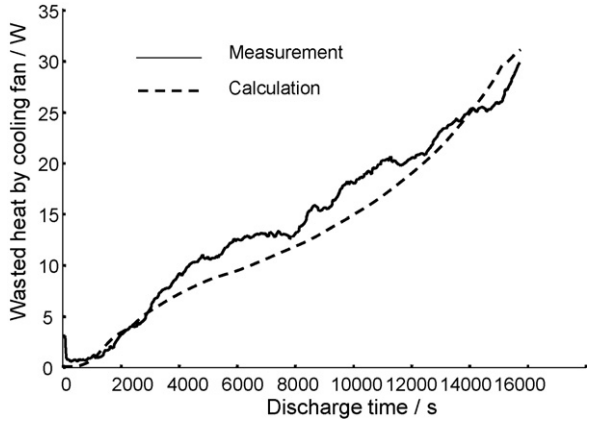

Fig. 7. Rate of heat removal from the battery module by cooling air. The solid line shows experimental data obtained by measuring the velocity of outlet air from the battery module and the temperature difference of the air between the inlet and outlet. The broken line is the calculation by the third term in Eq. (2).

4. Characteristics of weatherproof power supply system

4.1. Discharge and charge characteristics

The thermal design of the weatherproof power supply system in the discharging state was evaluated in a temperature control chamber. The power system was subjected to a temperature of 40 °C at 200 VA loading. One battery module was mounted in the system because this condition is the most severe in discharging due to constriction of the discharge current. As regards discharge, only the battery and inverter were working in the system, so they were the critical components for evaluating the thermal characteristics. The discharge was carried out after the thermal equivalent condition was reached in the state of full charge. Though it took 8 h to reach a steady state, the self-discharge capacity of the battery was small enough to be neglected. Since the inverter generated waste heat due to vampire energy in the standby mode, the thermal equilibrium temperature reached over 50 °C. Fig. 8 shows the discharge capacity, the temperature of the equipment, and the voltage of the battery module.

Cutoff voltage of 10 V was used for the battery module testing. Nevertheless, the value in the system depended upon the operation window of the inverter. The cutoff voltage of the inverter was regulated at 11.5 V, so the system stopped supplying power while the battery still had small capacity remaining. As a result, the discharge capacity of the battery was measured as 86 Ah (89%) in 40 °C ambient. Fig. 9 also shows the battery temperature profile during discharge. The cooling fan of the battery module is supposed to operate during charging and discharging if the temperature exceeds 45 °C. Thus, the cooling fan started to rotate as soon as the discharge had begun. Consequently, the battery temperature had decreased for several hours followed by temperature elevation. The current from the battery increased with decreasing voltage later in discharge.

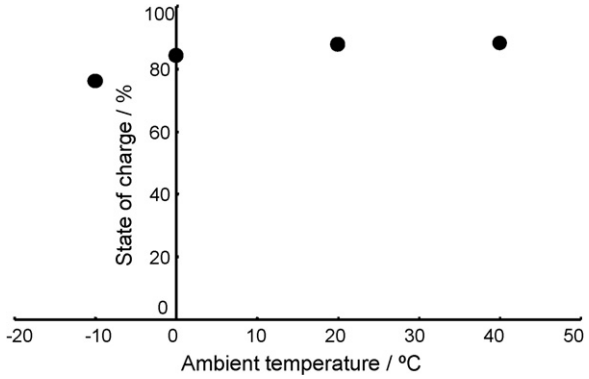

Fig. 9. Discharge capacity versus environmental temperature. Discharge capacity was obtained by changing ambient temperature in subsequent charge in the same condition where charge current is 20 A at room temperature.

The inverter was waiting in standby mode without driving its own cooling fan prior to discharge. The moment discharge started, the inverter started its cooling fan and the temperature started to decrease. Hence, we verified that the power system is useful for operation at high temperature. The discharge capacity depended on the ambient temperature, so that we obtained the capacity by changing the environmental temperature. Each measurement was carried out prior to the same charge condition in which the full charge satisfied dT/dt detection, rise in temperature of 1 °C every 5 min, at room temperature. Full charge was detected by monitoring the temperature of the battery rise with respect to time. The experimental result is shown in Fig. 9. The values in Fig. 9 indicate the SOC (state of charge) when full charge was 100%. Therefore, it is possible to discharge the power system under a wide temperature range, particularly in hot environments.

Following the discharge, the characteristics of the charge were obtained at 40 °C. Practically, charging should be done at lower ambient temperature, such as at nighttime temperatures or below 30 °C, to prevent acceleration of deterioration. However, in this study, the characteristics of the charge in high-temperature environment were measured to demonstrate performance of the battery. The battery was charged subsequent to the discharge at 200 VA loading. Fig. 10 shows the temperature and voltage of the battery module in the system at charging.

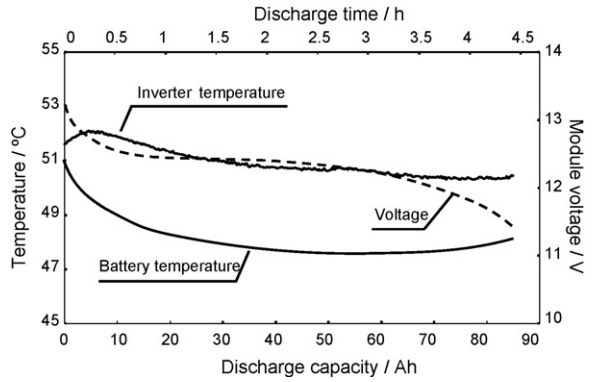

Fig. 8. Discharge characteristics of the battery module in the weatherproof power supply cabinet. In addition, temperature of inverter and battery during system operation is shown. The loading was 200 VA at 40 °C.

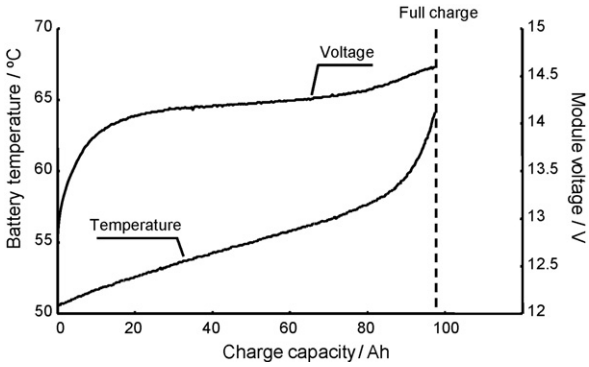

Fig. 10. Charge characteristics of the battery module in the weatherproof power supply cabinet. The charge current is 20 A at 40 °C. Full charge was detected by monitoring the temperature rise with respect to time, dT/dt detection.

Table 5
Environmental conditions in field test.

Ambient temperature	35 °C
Solar radiation intensity	750–900 W m^{-2} (800 W m^{-2} average)
Temperature on ground	50 °C

The temperature at the beginning of charge was over 50 °C. The charge completion to full charge, i.e., dT/dt detection, was observed even under this severe ambient condition. With conventional batteries, charging is difficult in environments of over 40 °C. The discharge capacity of the power system after charging under 40 °C environment was 85 Ah. Therefore, 88% of the charge capacities at 40 °C can be supplied at 200 VA loading in a 40 °C environment.

4.2. Thermal design evaluation on exposure to the sun

The thermal design of the system was evaluated by simulation based on an environmental field test. For the field test, the weatherproof power supply system was installed on the ground to expose it to sunlight on a hot summer day. The environmental conditions are shown in Table 5. The testing condition was more severe than the ordinary one for measuring the temperature of the power system. One battery module was mounted in the weatherproof power supply system to maximize the waste heat from the battery due to the maximum current flow. The loading power was 200 VA. Solar radiation intensity was measured with a pyranometer during the field test. The solar absorptivity and thermal emissivity of the cabinet surfaces had been measured prior to this test.

Two hours into the discharge test, solar radiation intensity reduced due to cloudiness, so the temperature estimation was carried out by analysis. The points of measured temperature were the inverter, the battery, inner air near the inverter, and the cabinet panels. In the experimental result, temperature profiles of the inner air and the cabinet panels showed similar behavior and values. Temperatures of the equipments at 200 VA loading are shown in Fig. 11.

If the temperature of atmosphere near the inverter exceeds 40 °C, its built-in cooling fan starts. The cooling fan began driving 0.7 h after the experiment start. After the cooling fan activated, the temperature of the inverter came to approximately the same temperature as the inner air. Furthermore, the temperature of the inner air was very sensitive to the temperature of the cabinet. Meanwhile, the cabinet temperature was determined from the heat balance on the cabinet surfaces. As shown in Fig. 11, the heat capacity of the battery module was large enough that the temperature elevated slowly. Following the experimental results in the temperature control chamber, it took 8 h to reach a steady state. Thus, the inverter

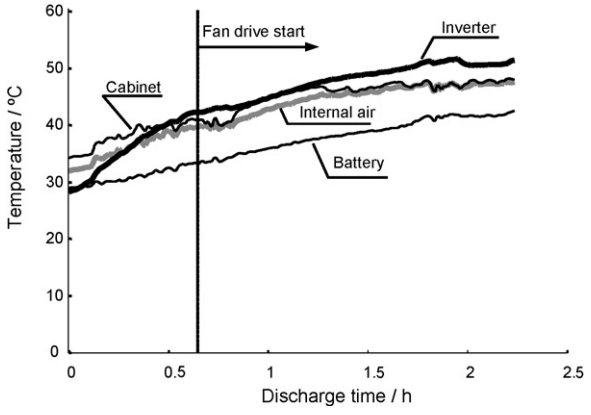

Fig. 11. Temperature of equipment in the system on exposure to sunlight. The system was operated at 200 VA loading on a hot day.

was more severe than the battery in discharge. The inverter temperature was calculated from an analysis until the end of discharge. The discharge duration is 5 h in the 1-module battery condition. First, we estimated the cabinet temperature by considering the thermal balance on the surface of the cabinet. The heat entering the cabinet was heat due to solar absorption, heat radiation from the ground, and the heat generated by the inverter and battery. The heat generated from the battery was calculated prior to pretesting according to the cubic spline interpolation of the temperature. Subsequently, the inverter temperature was predicted based on the cabinet temperature obtained by the previous calculation.

In the experimental results, the temperature differences between the four side panels of the cabinet were so small that the cabinet temperature was represented as the bulk temperature of the average of the four side panels. The thermal balance equations for the cabinet and inverter are

$$\mathrm{Cp_s}\frac{dT_s}{dt} + 4h_sA_p(T_s - T_\infty) + 4\sigma\varepsilon FA_p(T_s^4 - T_\infty^4) + Q_{grd} - Q_{sol} - Q_{in} = 0 \quad (12)$$

$$\mathrm{Cp_i}\frac{dT_i}{dt} + h_iA_i(T_i - T_s) + \mathrm{cp_a}\rho_a u_i A_{ia}(T_i - T_s) - Q_i = 0 \quad (13)$$

Eq. (12) describes the thermal balance of the system cabinet. The roof of the cabinet was covered with a sun shield panel to prevent solar energy entering the system. Thus, the main heat exchange occurred on the side panels of the cabinet. The heat inputs to the cabinet were heat due to solar absorption Q_{sol}, heat radiation from the ground Q_{grd}, and internal heat generated by the inverter and battery Q_{in}. The heat was removed from the cabinet by convection of external air and radiation to the ambient, the second term and the third term in Eq. (12), respectively. View factor, F, for radiation to ambience in the third term in Eq. (12) was assumed to be 0.5. Radiation from the system was conducted to the ground or ambient. As the ground area became larger, approaching infinity, the view factor between the panel and the ground approached 0.5. Hence, radiation to the ambient became the residual rate. Q_{grd} represents the heat radiation between the system cabinet and ground. However, the heat radiation rate from the ground obtained by analysis was as small as several watts, so it was possible to ignore this effect.

Eq. (13) expresses the thermal balance of the inverter. The cabinet temperature T_s estimated from Eq. (12) was substituted into Eq. (13) as the boundary temperature, because the temperature of the inner air for removing heat from the inverter was approximately equivalent to the cabinet temperature. The second term in Eq. (13) shows the heat transfer of the inverter surface, and third term is the rate of heat removal by the cooling fan built into the inverter.

The convection heat-transfer coefficients in Eqs. (12) and (13) were calculated regarding natural convection on a vertical or hori-

Table 6
Heat-transfer coefficient associated with Eqs. (12) and (13).

	Object	
	Inverter	System
Shape	Horizontal rectangular plate	Vertical rectangular plate
C	0.54	0.59
β	$1/(T_i + T_s)$	$1/(T_s + T_a)$
x	Horizontal length (w)	Vertical height (l)
Gr	$\frac{gw^3(T_i - T_s)}{\nu^2(T_i + T_s)}$	$\frac{gl^3(T_s - T_a)}{\nu^2(T_s + T_a)}$

Heat input	Description	Value
Q_{sol}	$I \times \cos\theta \times \alpha \times A_p$	106.7 W
Q_{in}	Heat from inverter (Q_i) (calculated by efficiency)	47 W
	Heat from battery (following Eqs. (1)–(3))	0–50 W

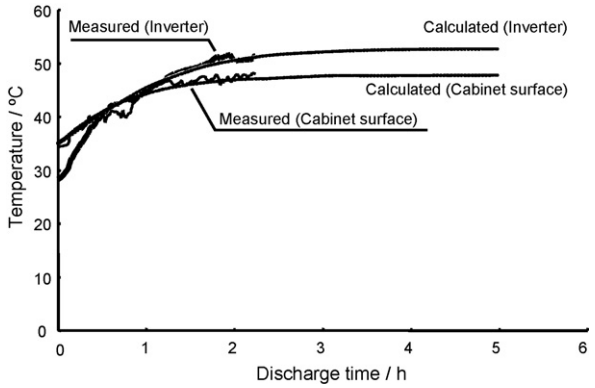

Fig. 12. Analysis results compared with measured temperature of equipment. Temperature was predicted by using Eqs. (12) and (13).

zontal surface as shown in Eq. (6). The parameter used in Eqs. (12) and (13) [including Eqs. (6) and (7)] are shown in Table 6.

Temperatures estimated for the inverter and cabinet by using Eqs. (12) and (13) are shown with measured data in Fig. 12.

The ambient temperature was assigned as the initial temperature for the analysis. From the estimation, it took over 3 h to reach the thermal equilibrium condition. The temperature of the inverter was predicted under the assumption that the cooling fan is driven. The cooling fan built into the inverter actually began to drive half an hour after discharge had started. Although the analysis temperature of the inverter was higher than the measured data at the beginning of the discharge, the two temperatures agreed well after the cooling fan was driven.

It was possible to estimate the temperature in the severe field testing in spite of the short hours. The validity of the model can be estimated during the transient before steady state of the temperature in field testing. The analysis and experimental results agrees during the transient. Therefore, the thermal analysis model is appropriate.

Therefore, the inverter in the system has enough allowable temperature margin, even if the environment condition becomes more severe than this field condition.

5. Conclusion

A weatherproof power supply system with nickel-metal hydride battery modules for stationary use was tested and its thermal characteristics were evaluated. The results are as follows:

(1) The developed battery was able to charge and discharge even in a 40 °C environment which means the power system can operate in a wide temperature range.
(2) In order to calculate the rate of heat generation from the battery module, a thermal mathematical model of the battery module was developed and measured temperature was approximated by a cubic spline interpolation. Because the heat removal rate in the analysis was within the error bounds of measured data, the thermal mathematical model is sufficient for estimating the heat generation rate of the battery. The discrepancy between measured temperature and analysis result obtained using the heat generation rate calculated with the cubic spline interpolation was insignificant, indicating that the cubic spline interpolation is appropriate for our numerical approach.
(3) The thermal design of the power system was verified by testing and analysis. The critical item for the power system is the inverter. The temperature was estimated by using the thermal equilibrium equation of the inverter. The equation was solved by using the boundary condition as the temperature of the cabinet panel obtained from the equation of the heat balance of the entire system. It was found that the inverter can be operated within the allowable temperature range at 200 VA loading on exposure to the sun in hot summer.

References

[1] K. Saito, T. Shodai, A. Yamashita, H. Wakaki, International Telecommunications Energy Conference, 2003, pp. 261–267.
[2] R. Kitano, A. Miyasaka, A. Yamashita, T. Shodai, International Telecommunications Energy Conference, 2007, pp. 614–620.
[3] L.T. Yeh, EEP-Vol. 23/HTD-Vol. 356, CAE/CAD and Thermal Management Issues in Electronics Systems, ASME, 1997, pp. 65–73.
[4] B. Ulrich, International Telecommunications Energy Conference, 1990, pp. 563–570.
[5] A.A. Pesaran, D.J. Russel, J.W. Crawford, R. Rehn, E.A. Lewis, 13th Annual Battery Conference on Applications and Advances, 1998, pp. 127–131.
[6] D. Pavlov, J. Power Sources 158 (2006) 964–976.
[7] D. Pavlov, B. Monahov, A. Kirchev, D. Valkonska, J. Power Sources 158 (2006) 689–704.
[8] S. Boyd, L. Jeongwoo, N. Douglas, Society of Automotive Engineering (Spec. Publ.), No. SP-2101, 2007, pp. 297–302.
[9] C. Bulle, A. Dupuy, ESA SP (Europe Space Agency), No. 288, 1988, pp. 449–455.
[10] M.M. Moorthi, International Telecommunications Energy Conference, 2003, pp. 112–118.
[11] S. Lansburg, J. McDowall, International Telecommunications Energy Conference, 2006, pp. 1–8.
[12] J.P. Holman, Heat Transfer, 9th edition, McGraw-Hill Higher Education, 2002, p. 292.
[13] J.P. Holman, Heat Transfer, 9th edition, McGraw-Hill Higher Education, 2002, p. 322.